

₁ Study of neutrino-nucleus interaction at around 1 GeV using
₂ a 3D grid-structure neutrino detector, WAGASCI, muon
₃ range detectors and magnetized spectrometer, Baby MIND,
₄ at J-PARC neutrino monitor hall

₅ A. Bonnemaison, R. Cornat, L. Domine, O. Drapier, O. Ferreira, F. Gastaldi,
₆ M. Gonin, J. Imber, M. Licciardi, F. Magniette, T. Mueller, L. Vignoli, and O. Volcy
₇ *Ecole Polytechnique, IN2P3-CNRS, Laboratoire Leprince-Ringuet, Palaiseau,*
₈ *France*

₉ S. Cao and T. Kobayashi

₁₀ *High Energy Accelerator Research Organization (KEK), Tsukuba, Ibaraki, Japan*

₁₁ M. Khabibullin, A. Khotjantsev, A. Kostin, Y. Kudenko, A. Mefodiev, O. Mineev,
₁₂ S. Suvorov, and N. Yershov

₁₃ *Institute for Nuclear Research of the Russian Academy of Sciences, Moscow, Russia*

₁₄ B. Quilain

₁₅ *Kavli Institute for the Physics and Mathematics of the Universe (WPI), The*
₁₆ *University of Tokyo Institutes for Advanced Study, University of Tokyo, Kashiwa,*
₁₇ *Chiba, Japan*

₁₈ T. Hayashino, A. Hiramoto, A.K. Ichikawa, K. Nakamura, T. Nakaya, K Yasutome,
₁₉ and K. Yoshida

₂₀ *Kyoto University, Department of Physics, Kyoto, Japan*

₂₁ Y. Azuma, J. Harada, T. Inoue, K. Kin, N. Kukita, S. Tanaka, Y. Seiya,
₂₂ K. Wakamatsu, and K. Yamamoto

₂₃ *Osaka City University, Department of Physics, Osaka, Japan*

²⁴ A. Blondel, F. Cadoux, Y. Favere, E. Noah, L. Nicola, and S. Parsa

²⁵ *University of Geneva, Section de Physique, DPNC, Geneva, Switzerland*

²⁶ N. Chikuma, F. Hosomi, T. Koga, R. Tamura, and M. Yokoyama

²⁷ *University of Tokyo, Department of Physics, Tokyo, Japan*

²⁸ Y. Hayato

²⁹ *University of Tokyo, Institute for Cosmic Ray Research, Kamioka Observatory,
30 Kamioka, Japan*

³¹ Y. Asada, K. Matsushita, A. Minamino, K. Okamoto, and D. Yamaguchi

³² *Yokoyama National University, Faculty of Engineering, Yokoyama, Japan*

³³ December 9, 2017

³⁴ 1 Introduction

³⁵ The understanding of neutrino-nucleus interactions in the 1 GeV energy region is critical
³⁶ for the success of accelerator-based neutrino oscillation experiments such as the T2K exper-
³⁷ iment. Complicated multi-body effects of nuclei render this understanding difficult. The
³⁸ T2K near detectors have been measuring these and significant progress has been achieved.
³⁹ However, the understanding is still limited. One of the big factors preventing from full
⁴⁰ understanding is the non-monochromatic neutrino beam spectrum. Measurements with
⁴¹ different but some overlapping beam spectra would greatly benefit to resolve the contri-
⁴² bution from different neutrino energies. We, the Wagasci collaboration, proposes to study
⁴³ the neutrino-nucleus interaction at the B2 floor of the neutrino monitor building, where
⁴⁴ different neutrino spectra can be obtained due to the different off-axis position. Our exper-
⁴⁵ imental setup contains 3D grid-structure plastic-scintillator detectors filled with water as
⁴⁶ the neutrino interaction target (Wagasci modules), two side- and one downstream- muon
⁴⁷ range detectors(MRD's). The 3D grid-structure and side-MRD's allows a measurement of
⁴⁸ wider-angle scattering than the T2K off-axis near detector (ND280). High water to scintil-
⁴⁹ lator material ratio enables the measurement of the neutrino interaction on water, which
⁵⁰ is highly desired for the T2K experiment because it's far detector, Super-Kamiokande,

51 is composed of water. The MRD's consist of plastic scintillators and iron plates. The
52 downstream-MRD, so called the Baby MIND detector, is also work as a magnet and pro-
53 vides the charge identification capability as well as magnetic momentum measurement for
54 high energy muons. The charge identification is essentially important to select antineu-
55 trino events in the antineutrino beam because contamination of the neutrino events is as
56 high as 30%. Most of the detectors has been already constructed. The Wagasci modules
57 have been commissioned as the J-PARC T59 experiment and the Baby MIND detector was
58 commissioned at the CERN neutrino platform. Therefore, the collaboration will be ready
59 to proceed to the physics data taking for the T2K beam time in January 2019. We will
60 provide the cross sections of the charged current neutrino and antineutrino interactions on
61 water with slightly higher neutrino energy than T2K ND280 with wide angler acceptance.
62 When combined with ND280 measurements, our measurement would greatly improve the
63 understanding of the neutrino interaction at around 1 GeV and contribute to reduce one
64 of the most significant uncertainty of the T2K experiment.

65 **2 Experimental Setup**

66 Figure. 1 shows a schematic view of the entire set of detectors. A central detector, Wagasci
67 modules, consists of 3D grid-structure plastic-scintillator detectors filled with water as the
68 neutrino interaction target. They are surrounded by two side- and one downstream- muon
69 range detectors(MRD's) The MRD's are used to select muon tracks from the charged-
70 current (CC) interactions and to reject short tracks caused by neutral particles that orig-
71 inate mainly from neutrino interactions in material surrounding the central detector, like
72 the walls of the detector hall, neutrons and gammas, or neutral-current (NC) interactions.
73 The muon momentum can be reconstructed from its range inside the detector. The MRD's
74 consist of plastic scintillators and iron plates. In addition, each of the iron plates of the
75 downstream-MRD, so called the Baby MIND detector, is wound by a coil and can be
76 magnetized. It provide the charge selection capability.

77 For all detectors, scintillation light in the scintillator bar is collected and transported
78 to a photodetector with a wavelength shifting fiber (WLS fiber). The light is read out by
79 a photodetector, Multi-Pixel Photon Counter (MPPC), attached to one end of the WLS
80 fiber. The signal from the MPPC is read out by the dedicated electronics developed for the
81 test experiment to enable bunch separation in the beam spill. The readout electronics is
82 triggered using the beam-timing signal from MR to synchronize to the beam. The beam-
83 timing signal is branched from those for T2K, and will not cause any effect on the T2K
84 data taking.

85 T2K adopted the off-axis beam method, in which the neutrino beam is intentionally
86 directed 2.5 degrees away from SK producing a narrow band ν_μ beam. The off-axis near
87 detector, ND280, is installed towards the SK direction in the B1 floor of the near detector
88 hall of the J-PARC neutrino beam-line. We propose to install our detector in the B2 floor

tmp.pdf

Figure 1: Schematic view of entire sets of detectors.

89 of the near detector hall, where the off-axis angle is similar but slightly different: 1.5 degree.
90 The candidate detector position in the B2 floor is shown in Fig. 2. The expected neutrino
91 energy spectrum at the candidate position is shown in Fig. 3.

92 **2.1 Wagasci module**

93 The dimension of the central detector is 100cm × 100cm in the x and y directions and
94 200cm along the beam direction. The total water and hydrocarbon masses serving as
95 neutrino targets are ~ 1 ton each. Inside the central detector, plastic scintillator bars are
96 aligned as a 3D grid-like structure, shown in Fig. 4, and spaces in the structure are filled
97 with the neutrino target materials, water and hydrocarbon. When neutrinos interact with
98 hydrogen, oxygen or carbon, in water and hydrocarbon, charged particles are generated.
99 Neutrino interactions are identified by detecting tracks of charged particles through plastic
100 scintillation bars. Thanks to the 3 D grid-like structure of the scintillator bars, the central
101 detector has 4π angular acceptance for charged particles. Furthermore, adopting a 2.5cm
102 grid spacing, short tracks originated from protons and charged pions can be reconstructed
103 with high efficiency. Thin plastic scintillator bars (thickness ~ 0.3 cm) will be used for the
104 central detector to reduce the mass ratio of scintillator bars to neutrino target materials,
105 because neutrino interactions in the scintillator bars are a background for the cross section
106 measurements. Scintillator bars whose dimensions are 2.5cm x 0.3cm x 100cm will be used
107 for the central detector. The total number of channels in the central detector is 12880.

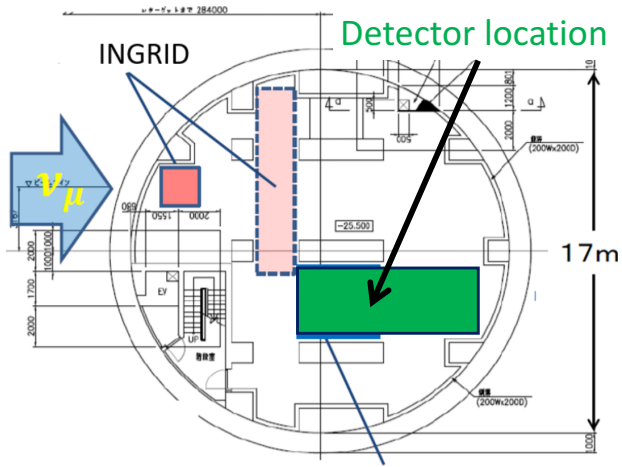


Figure 2: Candidate detector position in the B2 floor of the near detector hall.

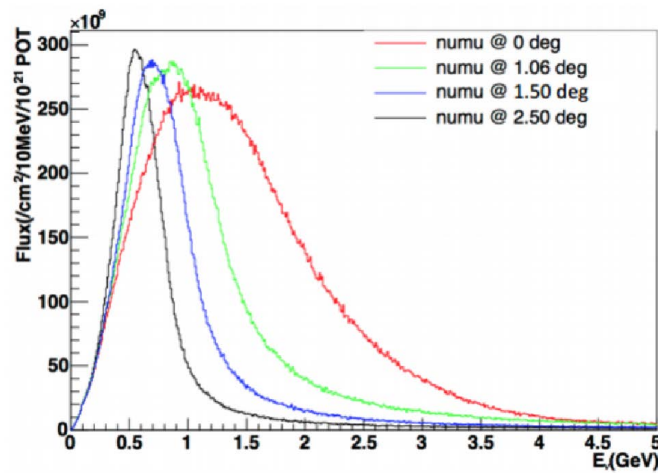


Figure 3: Neutrino energy spectrum at the candidate detector position(red, off-axis 1.5 degree). The spectrum at the ND280 site (black, off-axis 2.5 degree) is also shown.

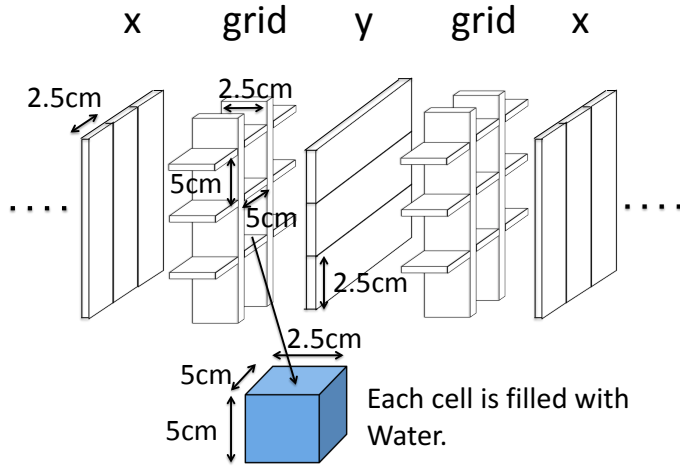


Figure 4: Schematic view of 3D grid-like structure of plastic scintillator bars inside the central detector.

¹⁰⁸ **2.2 Baby MIND**

¹⁰⁹ **2.3 Side muon range detector**

¹¹⁰ Four Side-MRD modules for tracking secondary particles from neutrino interactions will
¹¹¹ be constructed by the end of January 2018. Each Side-MRD module is composed of 11
¹¹² steel plates and 10 layers of total 80 scintillator slabs installed in 13 mm gaps between the
¹¹³ 30 mm thick plates. Each steel plate size is $30 \times 1610 \times 1800$ mm³. Total module size is
¹¹⁴ $2236 \times 1630 \times 975$ mm³ as shown in Fig. 5, weight is ~ 8.5 ton.

¹¹⁵ Scintillator bars were manufactured by Uniplast company in Vladimir, Russia. Polystyrene
¹¹⁶ based scintillators were extruded with thickness of 7 mm, then cut to the size of $7 \times 200 \times$
¹¹⁷ 1800 mm³. Dopant composition is 1.5% PTP and 0.01% POPOP. Scintillator surface was
¹¹⁸ etched by a chemical agent to form a white diffuse layer with excellent reflective perfor-
¹¹⁹ mance. Ideal contact between the scintillator and the reflector raises the light yield up to
¹²⁰ 50% comparing to an uncovered scintillator. Sine like groove was milled along the scin-
¹²¹ tillator to provide uniform light collection over the whole scintillator surface. WLS Y11
¹²² Kuraray fiber of 1 mm diameter is glued with an optical cement EJ-500 in the S-shape
¹²³ groove as shown in Fig. 6. Bending radius is fixed to 30 mm that was specified to be safe
¹²⁴ for Kuraray S-type fibers. Both ends of the fiber are glued into optical connectors (Fig. 7)
¹²⁵ which mounted within a scintillator body.

¹²⁶ The plastic molded connectors provide an interface to SiPMs, Hamamatsu MPPC
¹²⁷ S13081-050CS(X1) used for the WAGASCI detector. Optical coupler of this type (so-called

128 Baby-mind type of optical connector) consists of two parts (see Fig. 7): an container for
 129 the MPPC and a ferrule with the fiber. The ferrule is glued in the scintillator, and its end
 130 with glued in WLS fiber was polished. Both parts of the optical coupler are latched by a
 131 snap-like mechanism: a locking groove inside the container and matching ring protuber-
 132 ance on the ferrule. To ensure the optical contact a foam spring made of sponge rubber
 133 presses the MPPC to the fiber end (Fig. 8).

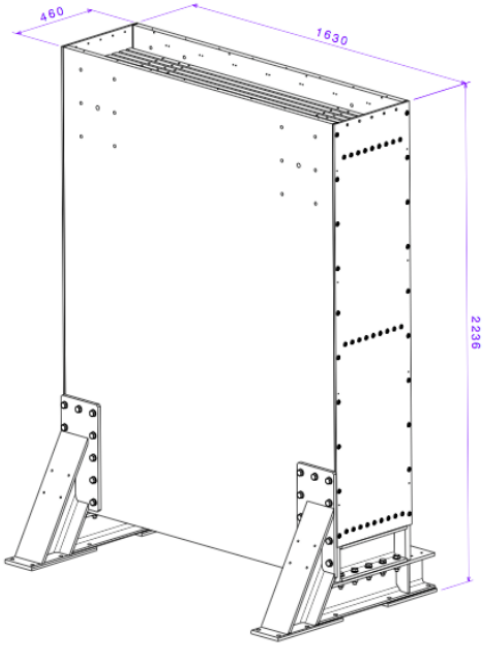


Figure 5: Support structure of the Side-MRD module.

134 Scintillators for the Side-MRD modules had been assembled at INR in Russia, and
 135 shipped to Japan in July 2017. The light yield for each scintillator was measured with
 136 cosmic rays at INR and at YNU in Japan after delivery. Parameters measured at the
 137 center of the counter were : the light yields LY_1 and LY_2 at both ends, the light yield
 138 asymmetry between the ends calculated as $100\% \times \frac{LY_1 - LY_2}{LY_1 + LY_2}$. After tests at INR we selected
 139 324 counters from measured 332 ones with the mean light yield of 45 p.e./MIP ($LY_1 + LY_2$
 140) and the asymmetry value less than 10 %. The measuremens at YNU yielded the average
 141 total light yield of about 40 p.e./MIP which varies in range from 32 to 50 p.e./MIP (Fig.
 142 9 (left)). Only two counters showed relatively high asymmetry close to 25 % as shown in
 143 Fig. 9 (right). Using the results of the quality assurance test we selected 320 scintillator
 144 counters for the Side-MRD modules.

145 We also measured the time resolution for a combination of four counters piled each on

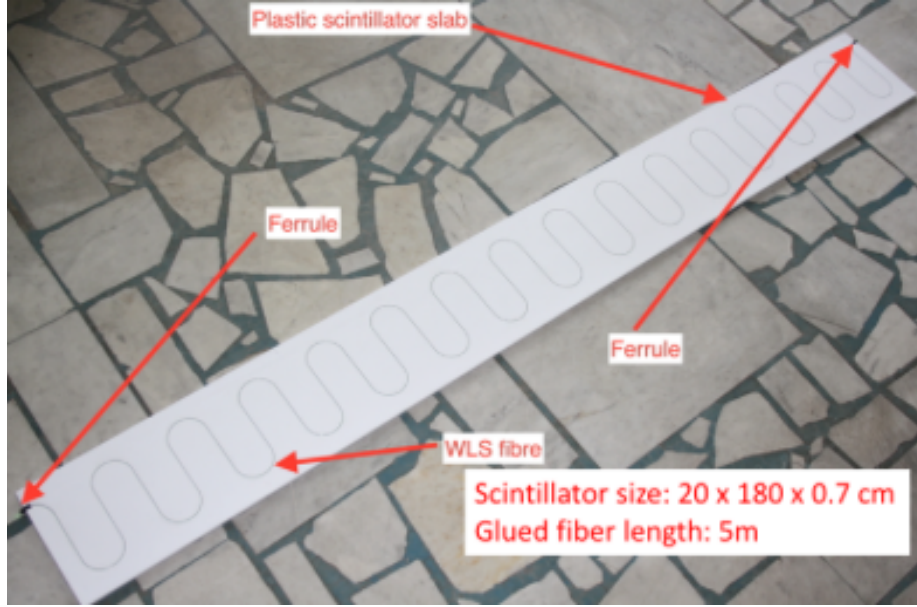


Figure 6: Scintillator bar of the Side-MRD modules.

another one. Time resolution for a single counter is determined as rms of $(T_{left} - T_{right})/2$ distribution. The difference of times was chosen to remove the correlated time fluctuation caused by a start trigger signal. The average result for four counters is $\sigma_T = 1.04$ ns (Upper left plot in Fig. 10). For a set of n counters the time resolution is calculated as $\frac{(T_L - T_R)_1 + (T_L - T_R)_2 + \dots + (T_L - T_R)_n}{2 \times n}$. The result of combination of 2, 3, 4 counters is 0.79 ns, 0.66 ns and 0.58 ns, correspondently (Fig. 10).

Construction of Side-MRD modules will be done from November 2017 to January 2018 at Yokohama National University, then they will be transported to J-PARC and will be installed at B2 floor of the T2K near detector hall before T2K beam in March 2018.

3 Physics goals

We will measure the differential cross section for the charged current interaction on H₂O and Hydrocarbon(CH)). The water-scintillator mass ratio of the Wagasci module is as high as 5:1 and the high purity measurement of the cross section on H₂O is possible. One experimental option is to remove water from one of the two Wagasci modules. The water-out WAGASCI module will allow to measure pure-CH target interactions with very low

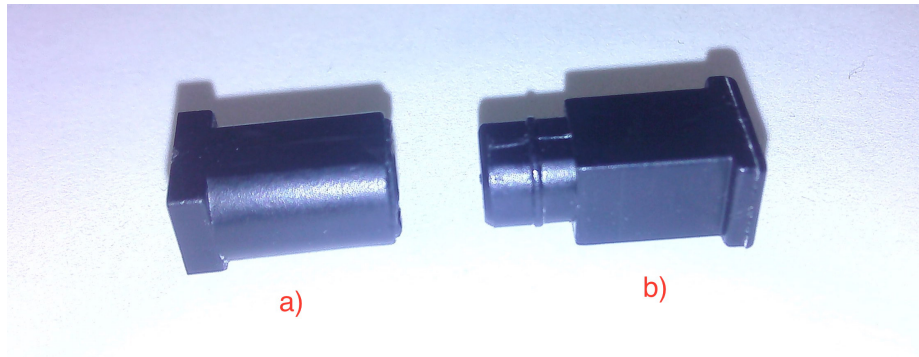


Figure 7: Optical connector for the Side-MRD scintillator. a) MPPC cover. b) Ferrule.

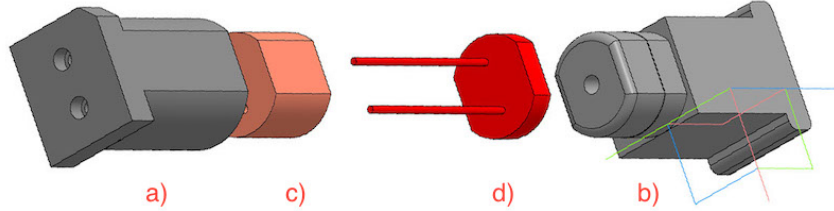


Figure 8: Scheme of the MPPC placement in optical connector. a) MPPC cover. b) Ferrule. c) Spring (sponge rubber). d) MPPC.

161 momentum-threshold for protons. It will also benefit to subtract the background from
 162 interaction with scintillator in the water target measurement. Another option is to add
 163 the T2K proton module which is fully made of plastic scintillators. It will allow the high
 164 statistics comparison of cross section between H₂O and CH and also comparison with
 165 the ND280 measurement. The actual configuration will be optimized with detailed MC
 166 simulation by 2018 Summer.

167 Our setup allows the measurements of inclusive and also exclusive channels such as 1- μ ,
 168 1- μ 1p, 1- μ 1 $\pi \pm np$ samples, former two of which are mainly caused by the quasi-elastic and
 169 2p2h interaction and the latter is mainly caused by resonant or coherent pion production
 170 and deep elastic scattering. In general, an accelerator produced neutrino beam spectrum
 171 is wide and the energy reconstruction somehow rely on the neutrino interaction model.
 172 Therefore, recent neutrino cross section measurement results including those from T2K
 173 are given as a flux-integrated cross section rather than cross sections as a function of
 174 the neutrino energy to avoid the model dependency. We can provide the flux-averaged

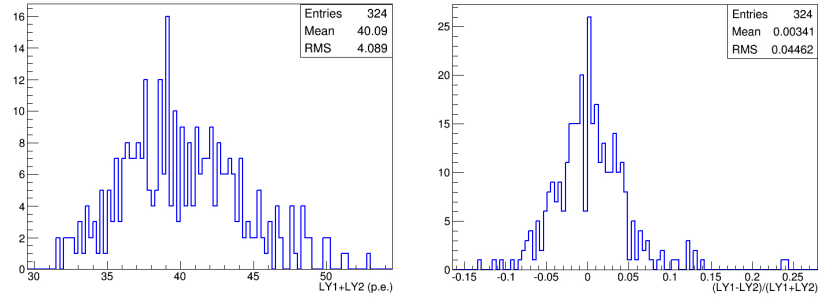


Figure 9: Total light yield distribution (left) and light yield assymetry (right) measured at YNU.

cross section. In addition, by combining our measurements with those at ND280, model-independent extraction of the cross section for narrow energy region becomes possible. This method was demonstrated in [1] and also proposed by P** (NUPRISM).

3.1 Expected number of events

Expected number of neutrino events after the event selections is evaluated with Monte Carlo simulations as we will discuss in Section 6. 2.41×10^4 CC events are expected in two WAGASCI modules after the selection with 1×10^{20} POT in neutrino-mode, and its purity is 75.5 %. In case we choose the option with one WAGASCI module and the T2K proton module, 1.2×10^4 CC events are expected in the WAGASCI module and $\sim 1 \times 10^4$ CC events are expected in the T2K proton module. In case we choose the option with one water-in WAGASCI module and one water-out WAGASCI module, 1.2×10^4 CC events are expected in the water-in module and 0.24×10^4 CC events are expected in the water-out module.

3.2 Pseudo-monochromatic beam by using different off-axis fluxes

The off-axis method gives narrower neutrino spectrum, and the peak energy is lower for larger off-axis angle. There still remains high energy tail mainly due to neutrinos from Kaon decay. The off-axis angle of the Wagasci location is 1.5 degree and different from the ND280 2.5 degree. Top two plots of Fig. 11 show the energy spectra of fluxes and neutrino interaction events at these two different location. The high energy tail of ND280 flux can be somehow subtraction by using the Wagasci measurement. The low energy part of the Wagasci flux can be also subtracted by using the ND280 measurement. Bottom two plots of Fig. 11 demonstrate this method. We can effectively get two fluxes, from 0.2 GeV to 0.9 GeV and 0.6 GeV and 2 GeV and measure flux-integrated cross section for these two



fig/side_mrd_combi_time.pdf

Figure 10: Time resolution for one (upper left) and a set of 2,3,4 Side-MRD counters.

198 fluxes.

199 **3.3 Subjects Wagasci can contribute**

200 In T2K experiment, neutrinos interact with bound nucleons in relatively heavy nuclei
201 (Carbon and Oxygen), so the cross-section is largely affected by nuclear effects. The nuclear
202 effects are categorized as nucleons' momentum distribution in nucleus, interactions with
203 correlated pairs of nucleons in nucleus (two particles-two holes, 2p2h), collective nuclear
204 effects calculated with Random Phase Approximation (RPA) and final state interactions
205 (FSI) of secondary particles in the nuclei after the initial neutrino interactions.

206 The 2p2h interactions mainly happen through Δ resonance interactions following a
207 pion-less decay and interactions with a correlated nucleon pair. The 2p2h interactions are

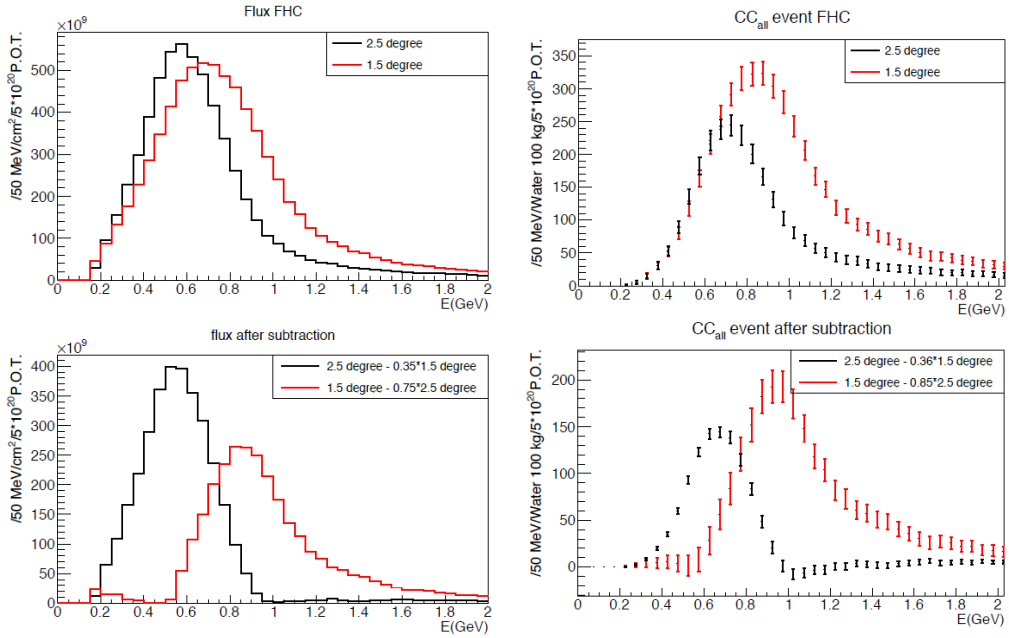


Figure 11: Energy spectra obtained by using different off-axis angle fluxes. Top two plots show the fluxes(left) and spectra of interaction events (right) for ND280 (off-axis 2.5 degree) and Wagasci (off-axis 1.5 degree). Bottom two plots show the fluxes (left) and spectra of interaction events (right) obtained by subtraction of fluxes at ND280 and Wagasci. The error bar is for the statistical error and those in the bottom right plot is obtained assuming the statistical error for ND280 measurement is much smaller than that of Wagasci experiment.

observed in electron scattering experiments (add ref. here) where the 2p2h events observed in the gap between Quasi-Elastic region and Pion-production region as shown in Fig. ???. Neutrino experiments also attempt to measure the 2p2h interactions, but separation of the QE peak and the 2p2h peak is more difficult because transferred momentum (p) and energy (w) are largely affected by neutrino energies which cannot be determined event-by-event in the wide energy spectrum of the accelerator neutrino beam. Our model-independent narrow neutrino spectra extracted from combined analyses of our data and ND280 data are ideal for searching the 2p2h interaction because clearer separation of the QE peak and the 2p2h peak is expected. Another way to observe the 2p2h interaction is direct measurement of proton tracks in CC π sample with low detection threshold and full acceptance. Fig. ?? shows proton multiplicities in CCQE events and 2p2h events, and Fig. ?? shows opening angles among two proton tracks in the same samples. The water-out WAGASCI can provide good sample for the 2p2h interaction search because its low density medium enables the

221 detection of low momentum protons in addition to the full acceptance.

222 The corrections from collective nuclear effects calculated by RPA as a function of Q^2 are
223 shown in Fig. ???. The Q^2 dependence of the correction can be tested by measuring angular
224 distribution of muons in CC1- μ and CC1- $\mu 1p$ events. The uncertainties of the corrections
225 in low (high) Q^2 regions can be constrained by observing the events with a forward-going
226 (high-angle) muon, so it is essential to measure muon tracks with full acceptance.

227 T2K experiment is starting to use ν_e CC1 π events for its CP violation search to increase
228 the statistics. One of the biggest uncertainty of the CC1 π sample comes from the final
229 state interactions of pions in the nuclei after the initial neutrino interactions because they
230 change the multiplicity, charge and kinematics of the pions. The multi-pion production
231 events can be migrated into the CC1 π sample due to the FSIs, and they become important
232 backgrounds. We can constrain the uncertainties from the pion FSIs by measuring pion
233 rescattering in the detector and pion multiplicity in ν_μ CCn π sample with low detection
234 threshold and full acceptance for pion tracks. The water-out WAGASCI can provide good
235 sample for the pion FSI studies because its low density medium enables the detection of
236 low momentum pions in addition to the full acceptance.

237 4 Status of J-PARC T59 experiment

238 We had submitted a proposal of a test experiment to test a new detector with a water
239 target, WAGASCI, at the T2K near detector hall to J-PARC PAC on April 2014, and the
240 proposal was approved as J-PARC T59. There are several updates on the project after
241 three years from then. Fist, the start time of neutrino beam measurement is changed from
242 December 2015 to October 2017, and the requested neutrino beam is changed from 1×10^{21}
243 POT of ν beam to 0.8×10^{21} POT of anti- ν beam. Second, the detector configuration is
244 changed. In the original proposal, central neutrino detector are expected to be surrounded
245 by newly developed muon-range detectors (MRDs), but we will use spare neutrino detectors
246 of the T2K experiment instead of them during neutrino beam measurement from October
247 to December 2017. Construction of the newly developed MRDs, Baby-MIND and Side-
248 MRD, is in progress, and they will be installed to the both sides and the downstream of
249 the central neutrino detector from January to March 2018. Then, we will resume neutrino
250 beam measurements from March 2018 and will take the neutrino beam data until May
251 2018.

252 4.1 On-axis beam measurement with Prototype detector

253 Add INGRID water module measurement here.

254 **4.2 Plans from October 2017 to May 2018**

255 J-PARC MR will extract its proton beam to T2K neutrino beam-line from October to
256 December 2017, and, from March to May 2018. T2K experiment will produce anti-neutrino
257 beam and will accumulate $\sim 8 \times 10^{20}$ POT data during the above period.

258 J-PARC T59 will perform neutrino beam measurements on the B2 floor of the T2K
259 near neutrino detector hall during the above period to test basic performances of the
260 WAGASCI detector and new electronics. During the beam measurements from October to
261 December 2017, one WAGASCI module will be placed between spare neutrino detectors of
262 the T2K experiment, INGRID Proton module and INGRID standard module. Here, the
263 INGRID Proton module is used as a charged particle VETO detector and, the INGRID
264 standard module is used as a downstream muon detector. We had submitted a proposal
265 to use these spare neutrino detectors for the T59 neutrino beam measurements to the T2K
266 collaboration, and we got an approval from T2K.

267 During the beam measurements from March to May 2018, Baby-MIND and two side
268 muon-range detector (Side-MRD) modules will be installed on the downstream and the
269 both sides of the WAGASCI detector, as shown in Fig. 12, to increase angular acceptance
270 for secondary charged particles from neutrino interactions. Add Baby-MIND commissioning
271 items here!!!

tmp.pdf

Figure 12: J-PARC T59 detector configuration with Baby-MIND and two Side-MRD modules from Mar. to May 2018. (Need to prepare the figure.)

272 Expected number of neutrino events in the WAGASCI detector during the above beam
273 period is evaluated with Monte Carlo simulations. Neutrino beam flux at the detector
274 location is simulated by T2K neutrino flux generator, JNUBEAM, neutrino interactions

275 with target materials are simulated by a neutrino interaction simulator, NEUT, detector
276 responses are simulated using GEANT4-based simulation. The neutrino flux at the detector
277 location, 1.5 degrees away from the J-PARC neutrino beam axis, is shown in Figure 3, and
278 its mean neutrino energy is around 0.68 GeV. An event display of the GEANT4-based
279 detector simulation is shown in Figure 15.

280 To perform the detector performance test, the following event selections are applied to
281 the data. First, track reconstructions are performed in the WAGASCI detector, and the
282 reconstructed vertex is required to be inside a defined fiducial volume, $80 \times 80 \times 32 \text{ cm}^3$
283 region at the center of the detector, to reduce contamination from external backgrounds.
284 Second, at least one charged particle is required to reach to INGRID standard module
285 or Side-MRD modules, and it makes more than two hits in these sub-detectors. With the
286 event selection, expected numbers of the neutrino-candidate events during the beam period
287 are summarized in Table 1. Using the data, we will test the detector performance with
288 $\sim 3\%$ statistical uncertainties.

289 5 Detector performance

290 5.1 Wagasci module

291 To demonstrate the performance of the Wagasci module and also to study the neutrino
292 interaction, the first Wagasci module was installed at the on-axis position, in front of
293 the T2K INGRID horizontal center module in 2016. The INGRID module is made of iron
294 plates and segmented plastic scintillator bars. It's cross sectional size viewed from the beam
295 direction is $1 \text{ m} \times 1 \text{ m}$. The charged current interactions in the Wagasci module are selected
296 by requiring a muon track candidate in the INGRIRD modules. Here, we describe the
297 performance of the Wagasci module evaluated at this T2K on-axis measurement. Figure 13
298 shows the light yeild of channels for muons produced by the interaction of neutrinos in the
299 hall wall. The light yield is sufficiently hgh to get good hit efficieincy. A track search
300 algorithm based on the cellular automaton has been developed using the software tools by
301 the T2K INGRID. The tracking efficiency in 2-dimentional projected plane was evalualted
302 by comparing the reconstructed track in the Wagasci module and the INGRID module and
303 shown in Fig.14. Note that that the tracking efficinecy for high angle ($> 70 \text{ deg}$) is not
304 evaluated because of the acceptance of the INGRID module, not because of the limitation
305 of the Wagasci module.

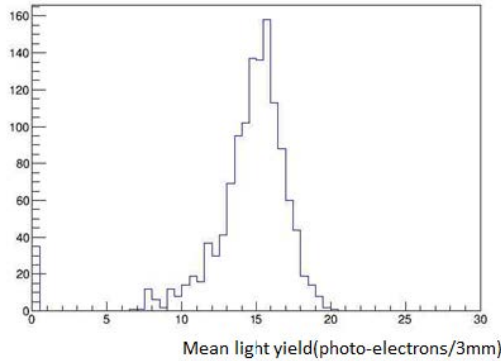


Figure 13: Light yield of channels for muons produced by the interaction of neutrinos in the hall wall.

306 **5.2 Baby MIND**

307 **5.3 Side muon range detector**

308 **6 MC studies**

309 **6.1 Detector simulation**

310 Expected number of neutrino events in the WAGASCI detector is evaluated with Monte
 311 Carlo simulations. Neutrino beam flux at the detector location is simulated by T2K neutrino
 312 flux generator, JNUBEAM, neutrino interactions with target materials are simu-
 313 lated by a neutrino interaction simulator, NEUT, detector responses are simulated using
 314 GEANT4-based simulation. The neutrino flux at the detector location, 1.5 degrees away
 315 from the J-PARC neutrino beam axis, is shown in Figure 3, and its mean neutrino energy
 316 is around 0.68 GeV.

317 **6.1.1 Detector geometry**

318 The detector geometry in the GEANT4-based simulation is slightly different from the
 319 actual detector as shown in Fig. 17. The active neutrino target region consists of four
 320 WAGASCI modules, and each WAGASCI detector has the dimension with 100 cm \times 100
 321 cm in the x and y directions and 50 cm along the beam direction. An event display of a
 322 MC event in the WAGASCI detectors is shown in Figure ???. Two Side-MRD modules is
 323 installed at both sides of the WAGASCI modules, and each Side-MRD module consists of
 324 ten iron plates whose dimension is 3 cm (thickness) \times 180 cm (height) \times 320 cm (width).
 325 The distance between the Side-MRD modules and WAGASCI modules is 60 cm. The

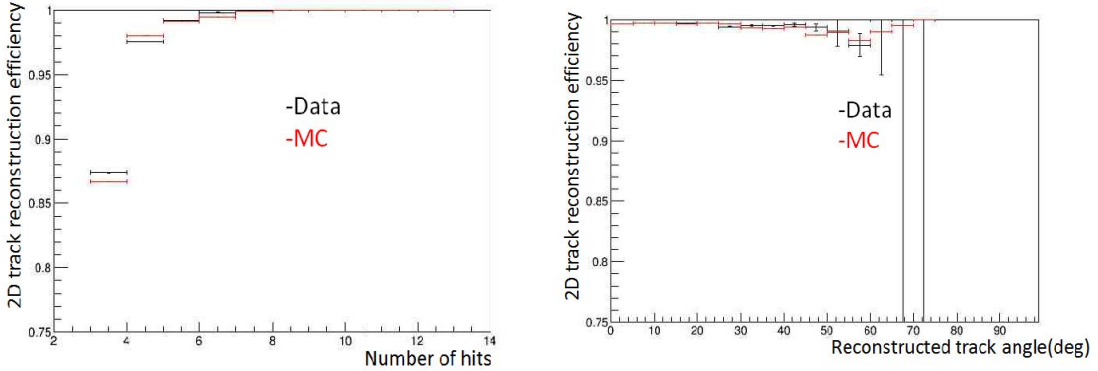


Figure 14: 2D track reconstruction efficiency as a function of number of hits (left) and track angle (right). Here the track angle is the one reconstructed by the INGRID module.

326 downstream-MRD equivalent to the Baby-MIND is installed at the downstream of the
 327 WAGASCI modules. The downstream-MRD consists of ten iron plates whose dimension is
 328 3 cm (thickness) \times 180 cm (height) \times 320 cm (width) and another ten iron plates whose
 329 dimension is 6 cm (thickness) \times 180 cm (height) \times 320 cm (width). The distance between
 330 the downstream-MRD modules and WAGASCI modules is 60 cm.

331 In order to estimate backgrounds from neutrino interactions in the wall and floor of the
 332 experimental hall, the geometry of the experimental hall is implemented in the GEANT4-
 333 based detector simulation.

334 6.1.2 Response of detector components

335 The energy deposit inside the scintillator is converted into the number of photons. The
 336 effects of collection and attenuation of the light in the scintillator and the WLS fiber are
 337 simulated, and the MPPC response is also taken into account. The light yield is smeared
 338 according to statistical fluctuations and electrical noise.

339 6.2 Track reconstruction

340 To select neutrino interaction from the hit patterns, a track reconstruction algorithm is
 341 developed. The flow of the track reconstruction is as follows.

- 342 1. Two-dimensional track reconstruction in each sub-detectors
- 343 2. Track matching among the sub-detectors
- 344 3. Three -dimensional track reconstruction

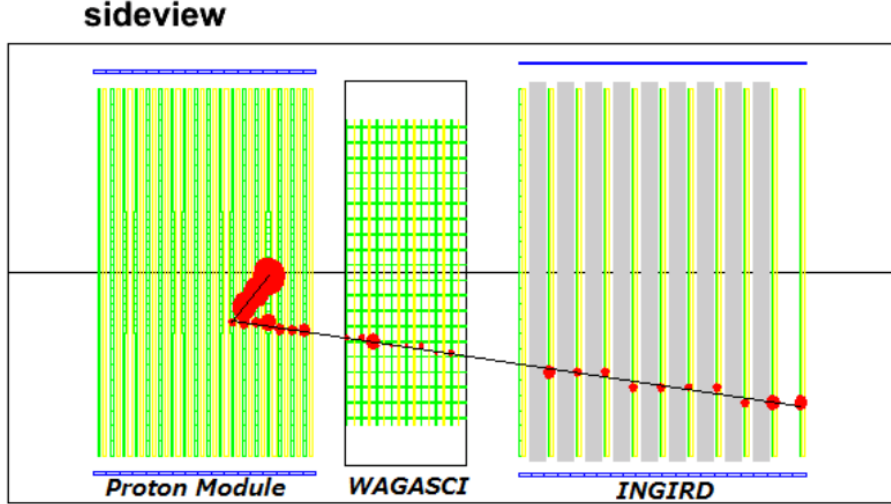


Figure 15: J-PARC T59 event display of a neutrino event in the GENAT4-based detector simulation.

345 Add explanation about two-dim reco, track matching and three-dim reco here.

346 6.3 Event selection

347 First, the events with the track which starts in 5 cm from the wall of the WAGASCI module
 348 are rejected to remove the background from the outside.

349 Second, to reject backgrounds from NC and neutral particles, the longest tracks are
 350 required to penetrate more than one (five) iron plates in Side-MRD modules (Baby-MIND).
 351 Then, in order to measure muon momentum, the longest tracks are required to stop in
 352 MRDs (Side-MRD modules and Baby-MIND) or penetrate all iron plates.

353 Table 1 and 2 show numbers of the selected events after each event election in neutrino-
 354 mode and antineutrino-mode respectively. As for the neutrino-mode, 2.12×10^4 CC events
 355 are expected with 1×10^{21} POT, and the purity is 81.3 %. The main background for
 356 the neutrino-mode is the neutrino interactions in the scintillators inside the WAGASCI
 357 detector. As for the antineutrino-mode, 0.83×10^4 CC events are expected with $1 \times$
 358 10^{21} POT, and the purity is 62.0 %. The main background for the antineutrino-mode
 359 is the wrong sign contamination from ν_μ events and the antineutrino interactions in the

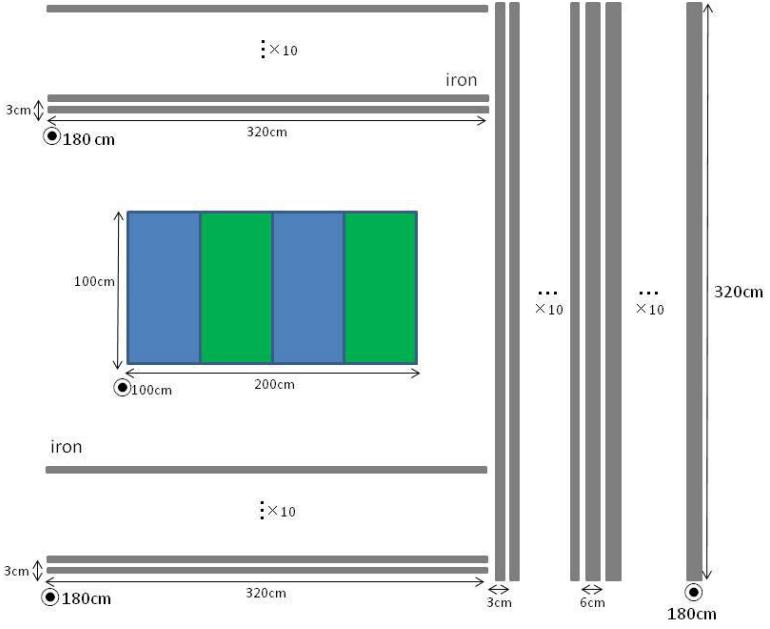


Figure 16: Geometry of the detectors in the Monte Carlo simulation.

360 scintillators inside the WAGASCI detector.

361 Figure 18 and 19 show the reconstructed angles of the longest tracks in the selected
362 events in the neutrino-mode and the anti-neutrino mode respectively.

363 Figure 20 and 21 show the iron plane numbers corresponding to the end points of the
364 longest tracks in the selected events.

365 6.4 Cross section measurements on water

366 In the water target events, the background from interaction with scintillators has to be
367 subtracted by using the measurement of the hydrocarbon target.

368 6.4.1 Charged current cross section measurement

369 7 Standalone WAGASCI-module performances

370 In the previous sections, the WAGASCI detector was studied using the Muon Range De-
371 tectors. In this section, the standalone abilities of WAGASCI module are presented. Using
372 the WAGASCI configuration presented in Section 6, we have evaluated that only 7% of

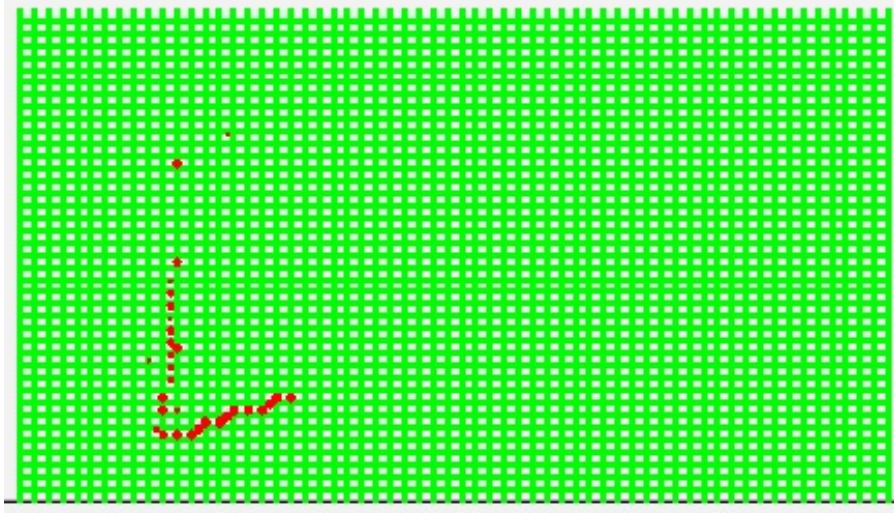


Figure 17: An event display of MC event in WAGASCI detectors. Green lines are scintillators and red circles are the hit channels.

373 the muons will be stopped in one of the WAGASCI modules. THowever, this proportion
 374 increases to 53% for pions and 73% for protons produced by neutrino interactions at 1.5°
 375 off-axis. Figure 22 shows the momentum distribution of these daughter particles as well as
 376 for the sub-sample stopped in one of the WAGASCI modules. Therefore, the study of the
 377 standalone abilities of the WAGASCI module in this section are dominantly motivated by:

- 378 • the accurate measurement of the neutrino interaction final states. Though most of the
 379 muons will be reconstructed and identified in the MRDs, the hadronic particles will
 380 predominantly stops in one WAGASCI module. One has therefore to rely exclusively
 381 on the WAGASCI module information alone to reconstruct, identify and measure the
 382 momentum of pions or protons.

Table 1: Expected number of the neutrino-candidate events in two WAGASCI modules after the event selections with 1×10^{21} POT in neutrino-mode.

Cut	CC	NC	Scinti Bkg.	Total
Reconstructed	45233	1749.27	9396.46	56378.8
FV	37876.8	1471.02	7869.57	47217.4
Pene. iron	28160.7	593.267	5750.79	34504.7
Stop/Penetrate MRDs	21195.4	534.914	4346.06	26076.4
after all cuts	81.3 %	2.1 %	16.7 %	100 %

Table 2: Expected number of the antineutrino-candidate events in two WAGASCI modules after the event selections with 1×10^{21} POT in antineutrino-mode.

Cut	CC	NC	Scinti Bkg.	Wrong sign bkg	Total
Reconstructed	16249.1	268.082	4468.83	5826.95	26813.0
FV	13644.7	223.211	3746.85	4866.36	22481.0
Pene. iron	10430.8	76.9422	2881.81	3901.35	17290.9
Stop/Penetrate MRDs	8328.73	71.2382	2240.59	2802.98	13443.5
after all cuts	62.0 %	0.5 %	16.7 %	20.9 %	100 %

- the coverage of the MRDs is not 4π . Using the WAGASCI module information can therefore help to constraint the particles that exits the WAGASCI module but do not geometrically enters any MRD.
- the particle identification of low momenta muons $p_\mu < 300$ MeV/c that will leave only few hits in the MRD. Using the WAGASCI module information will clearly enhance the particle identification.

This study is based on an original study done for the ND280 upgrade target, with some modifications. Though the cell size is similar to the WAGASCI configuration presented in Section 6, the external dimensions are different ($186.4 \times 60 \times 130$ cm 3). Whenever the results are presented with this external size and this parameter is likely to impact the result, it will be mentioned.

Note that in this section, a simplified reconstruction algorithm presented in Section 7.1 is used. The fiducial volume is chosen accordingly as the inner cube of the module which surfaces are distant of $4 \times$ scintillator space = 10 cm from the module external surfaces. The neutrino interactions are simulated using NEUT v5.3.2. The NEUT input neutrino flux is estimated using JnuBeam v13a and assuming the detector to be located at 1.5° off-axis, as in Section 6. Note that the event reconstruction efficiency as a function of true neutrino energy might be changed at 1.5° , due for example to different Q^2 distributions. For this reason, one has to note that the reconstruction results might slightly be changed from 2.5° and 1.5° . To avoid a similar change on the particle-only reconstruction efficiencies, they will be presented as a function of variables that completely characterize the particle kinematic state, *i.e.* its momentum and angle. Figure 23 shows the vertices distributions of the daughter particles of neutrinos interacting one standard WAGASCI water-module. In this section, we will show the detector reconstruction and particle identification in this phase space, both for leptonic and hadronic particles. We will finally show an empty WAGASCI module can highly enhance the ability to constrain the neutrino interaction final state which is critical to reduce the corresponding uncertainties.

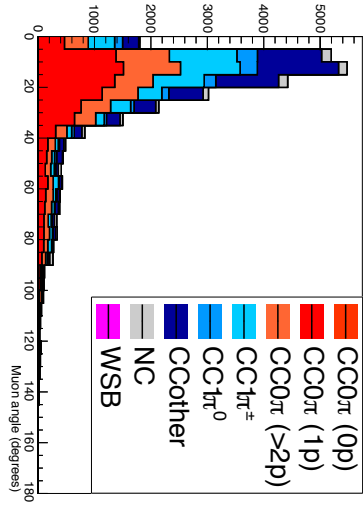


Figure 18: The reconstructed angles of the longest tracks in the selected events in the neutrino-mode.

410 **7.1 Reconstruction algorithm**

411 **7.1.1 Description**

412 For this section, an ideal “simulated” reconstruction is developed. A particle is recon-
413 structed if:

- 414 1. The particle is charged.
415 2. Lets at least one hit (energy deposit > 2.5 photo-electron) in a scintillator.
416
417 3. The particle enters one TPC and let one hit in the tracker.
418 Or

- 419
420 • The particle should be long enough to be reconstructed by the detector in at
421 least 2 out of 3 views (XZ, YZ, XY). The length criterion requires the particle
422 to let at least 4 hits in the detector. In the “less favourable case” of pure
423 longitudinal or transverse going tracks, it represents a the track length of $L_{track} \geq$
424 $4 \times$ scintillator space = 10.0 cm.
425 • In the views where particles pass the length criterion, the particle shall not
426 be superimposed with longer tracks in at least two views. The superposition

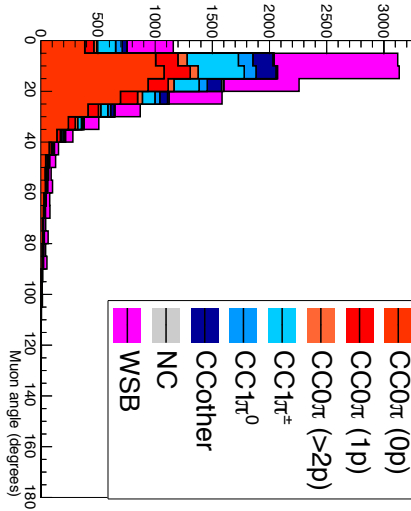


Figure 19: The reconstructed angles of the longest tracks in the selected events in the antineutrino-mode.

427 criterion is estimated with the distance inter-tracks (DIT) which corresponds to
 428 the orthogonal distance between two tracks at the ending point of the shortest
 429 one (see Figure 24). For a track 1, the superposition criterion is tested with
 430 every longer tracks that starts at the same vertex. Let \vec{p}_1 the vector of track
 431 1, and p_1^a its projections in the XZ, YZ and XY planes respectively for $i=1,2,3$.
 432 Note that these are projections in a 2D planes and not on a direction vector. In
 433 this case, the relative angle between the track 1 and a longer track 2 (of vector
 434 \vec{p}_2) in a view a is given by:
 435

$$\cos \theta = \frac{\vec{p}_1^a \cdot \vec{p}_2^a}{\|\vec{p}_1^a\| \|\vec{p}_2^a\|} \quad (1)$$

and the distance inter track is given by:

$$DIT = \|\vec{p}_1^a\| \sin \theta \quad (2)$$

436 The DIT should be higher than $4 \times$ scintillator width for the track 1 to be not
 437 superimposed with the track 2 in the view a, which also corresponds to 10.0 cm
 438 in the nominal configuration.

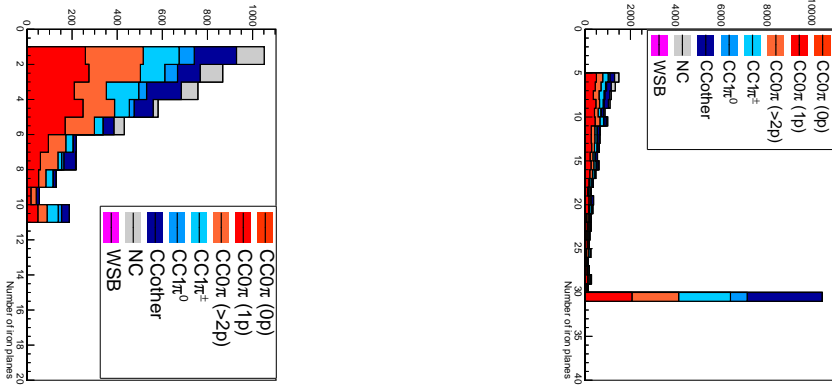


Figure 20: Iron plane numbers in Side-MRD (left) and Baby-MIND (right) corresponding to the end points of the longest tracks in the selected events in the neutrino-mode.

439 7.1.2 Performances

440 The particle-only reconstruction efficiencies and the reconstruction threshold in momenta
 441 are shown in Table 3. This threshold is defined as the maximal momentum for which the
 442 reconstruction efficiency is smaller than 30%. The thresholds in muon and pion momenta
 443 are 150 MeV/c. Most of the muons are above this threshold (see Figure 23) which leads
 444 to a 79% reconstruction efficiency.

	μ	π	p
Reconstruction Efficiency	79%	52%	26%
Momentum threshold	150 MeV/c	150 MeV/c	550 MeV/c

Table 3: Reconstruction efficiency and momentum threshold for muons, pions and protons. The threshold is defined as the maximal momentum for which particles have a reconstruction efficiency smaller than 30%.

445 The lower pion and proton efficiencies (respectively 52% and 26%) are due to lower
 446 efficiencies for similar momenta than muons, coming from strong interactions as shown
 447 on Figures 25. Efficiencies of each particle type tend to decrease in the backward region
 448 due to particle lower momenta. However, for a fixed momentum value, the reconstruc-
 449 tion efficiency is almost uniform which confirms the ability of the WAGASCI detector to
 450 reconstruct high angle tracks.

451 The reconstruction is thereafter tested on neutrino events. Table 4 summarizes the
 452 number of reconstructed events and efficiencies for each interaction type. As expected

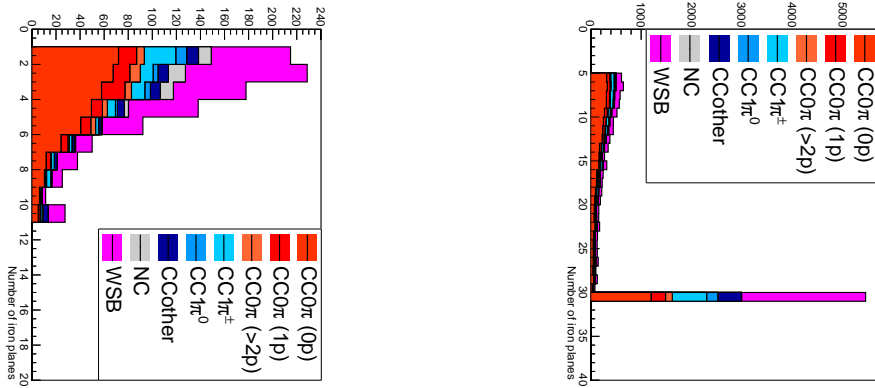


Figure 21: Iron plane numbers in Side-MRD (left) and Baby-MIND (right) corresponding to the end points of the longest tracks in the selected events in the antineutrino-mode.

453 from the high muon reconstruction efficiency, the charged current interactions have reconstruction
 453 efficiencies $\geq 85\%$.

	CC0 π	CC1 π	CCOthers	NC	All
Reconstruction efficiency	85%	87%	91%	22%	68%

Table 4: Number of true interactions reconstructed. The purity and reconstruction efficiency of each true interaction is also shown.

454
 455 The reconstruction efficiencies as a function of the neutrino energy and muon kinematics
 456 are respectively shown on Figure 26 and 27.

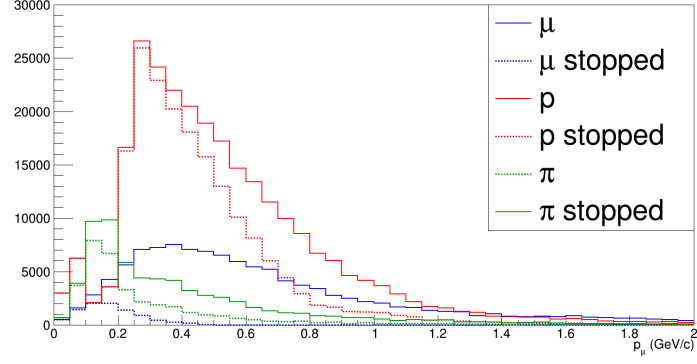


Figure 22: Momentum distribution of true particles in WAGASCI (plain) and corresponding distributions only for particles stopping into the WAGASCI module (dashed).

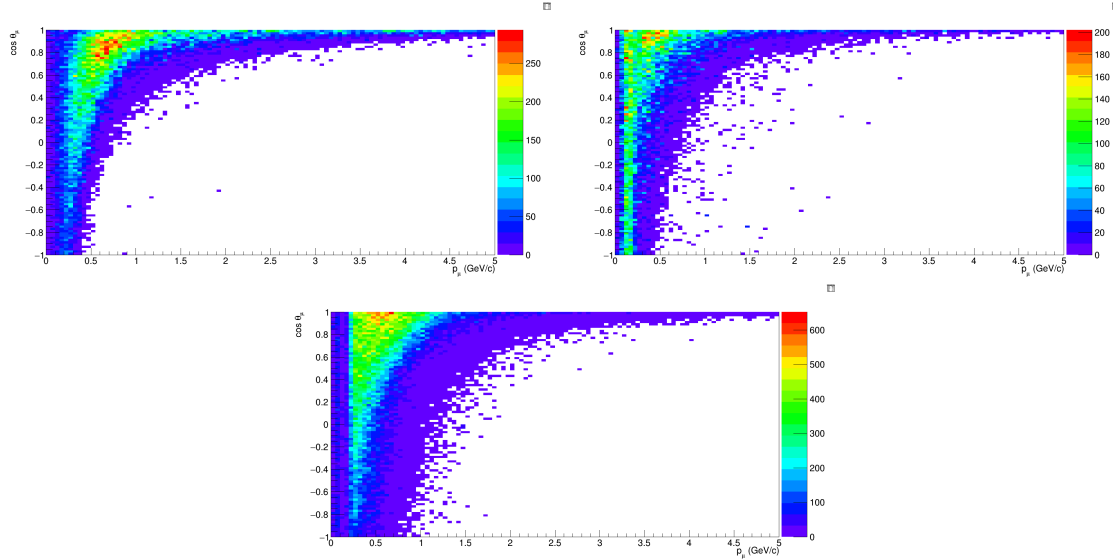


Figure 23: True number of muons (left), charged pions (right) and protons (bottom) in the two WAGASCI water-module as a function of the particles momenta and angles at 1.5° .

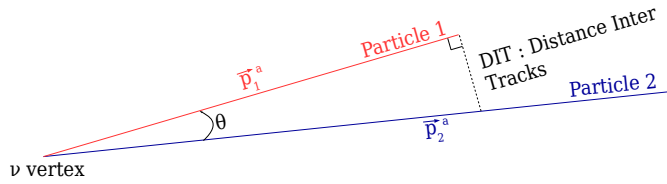


Figure 24: Definition of the distance inter tracks.

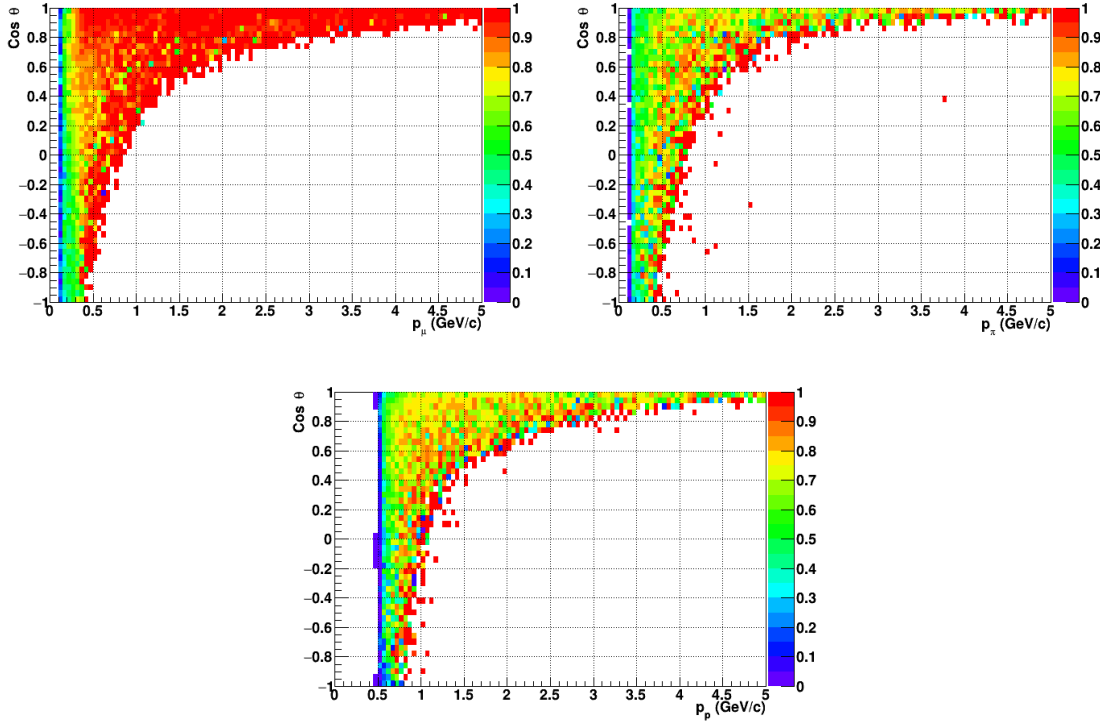


Figure 25: Reconstruction efficiency of muons (left), charged pions (right) and protons (bottom) in the WAGASCI water-module as a function of the particles momenta and angles.

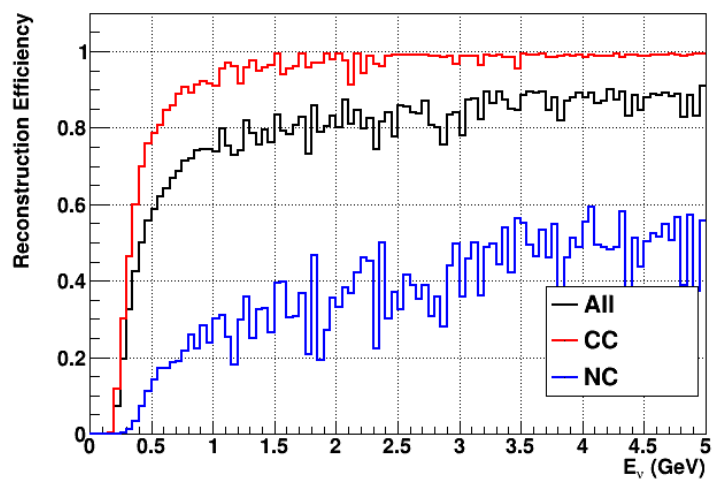


Figure 26: Reconstruction efficiency of all neutrino (black), CC (red) and NC (blue) interactions in the WAGASCI water-module as a function of the neutrino energy.

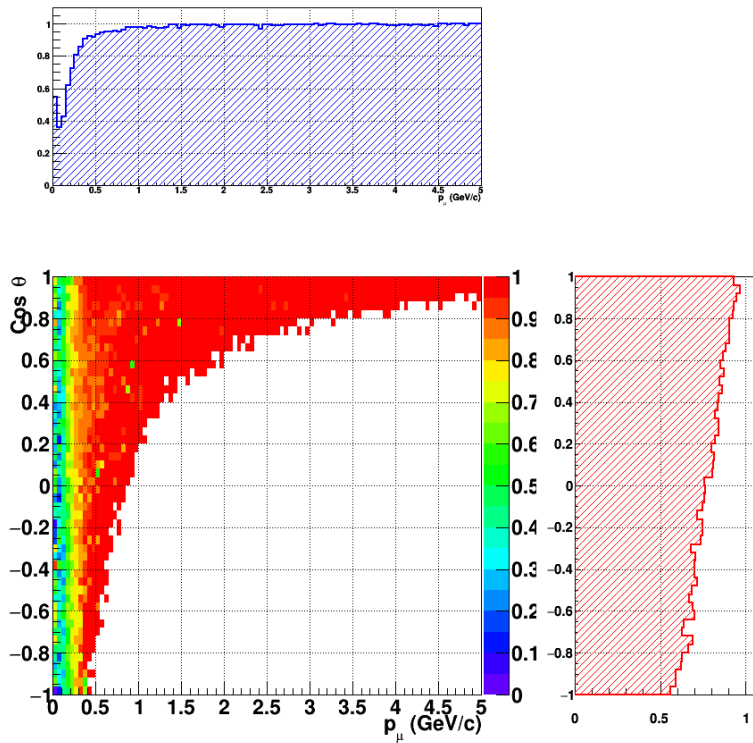


Figure 27: Reconstruction efficiency of CC interactions in the WAGASCI water-module as a function of the muon kinematic variables (momentum and angle).

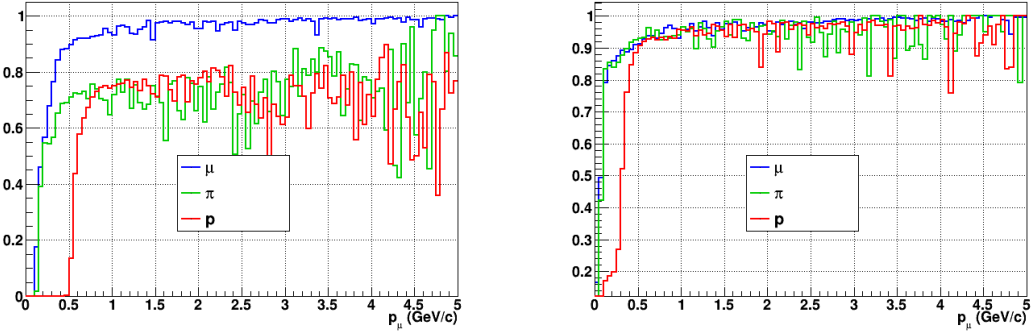


Figure 28: Reconstruction efficiency for muons, pions and protons in the water-in (left) and water-out (right) modules.

457 Note that a Particle Identification Algorithm has been also developed. It is based on
 458 the charge deposition of the particles in the scintillator, of the detection of a decay-electron.
 459 However, this information highly depends on the number of scintillator hit by a particle,
 460 which creates an important difference between a real WAGASCI module and the one used
 461 for the ND280-upgrade simulation. For this reason, the corresponding results will not be
 462 detailed here, but can be found in [?].

463 7.2 Background subtraction: the water-out module

464 In the nominal configuration, 20% of the neutrino interactions occurs on scintillators
 465 (C_8H_8). This background should be removed in order to measure the neutrino interac-
 466 tion on the same target as Super-K, which suppress the differences in cross-section models.
 467 For this purpose, we propose to use a water-out module, where the water is replaced by
 468 air. The detector is therefore fully active and has a 3 mm spatial resolution (scintillator
 469 thickness) which create an ideal detector to reconstruct and identify hadrons, and study
 470 np-nh interactions. The counter-part is the difference in particle energy deposition between
 471 the water and this water-out module that will need to be corrected for. In this section,
 472 we present the capabilities of such a module, and the impact it can have on cross-section
 473 measurements for the neutrino community in general and T2K in particular.
 474 The same reconstruction and selection as the water-in module is applied. Figure 28 shows
 475 the comparison between the water-in and the water-out reconstruction efficiencies for muon,
 476 pions and protons. 90% of the muons and 87% of the pions are reconstructed, while 70%
 477 of the protons are even reconstructed. It allows to lower down the proton threshold to
 478 250 MeV/c (see Table 5).

479 As a consequence of tracking even low momenta particle, the reconstruction efficiency
 480 is uniform and almost maximal on the entire $\cos \theta_\mu$ phase space, as shown on Figure 29.

	μ	π	p
Reconstruction Efficiency Momentum threshold	90% 50 MeV/c	87% 50 MeV/c	70% 250 MeV/c

Table 5: Reconstruction efficiency, proportions of μ -like and non μ -like and momentum threshold for muons, pions and protons in the empty module. The threshold is defined as the maximal momentum for which particles have a reconstruction efficiency smaller than 20%.

481 Since the fiducial mass represents 0.25 tons, the total number of events is divided by a
 482 factor of 3 compared to the water-in module. The water-out module offers interesting
 483 possibilities to study np-nh interaction since 70% of the protons are reconstructed. In the
 484 future, a possible separation as a function of the number of proton track will be studied.
 485 Moreover, we are currently pursuing the use of single and double transverse variables (cite
 486 Xianguo) to open new possibilities for separating np-nh from Final State Interactions, or
 487 for isolating the interactions on hydrogen from interactions on carbon in this module.

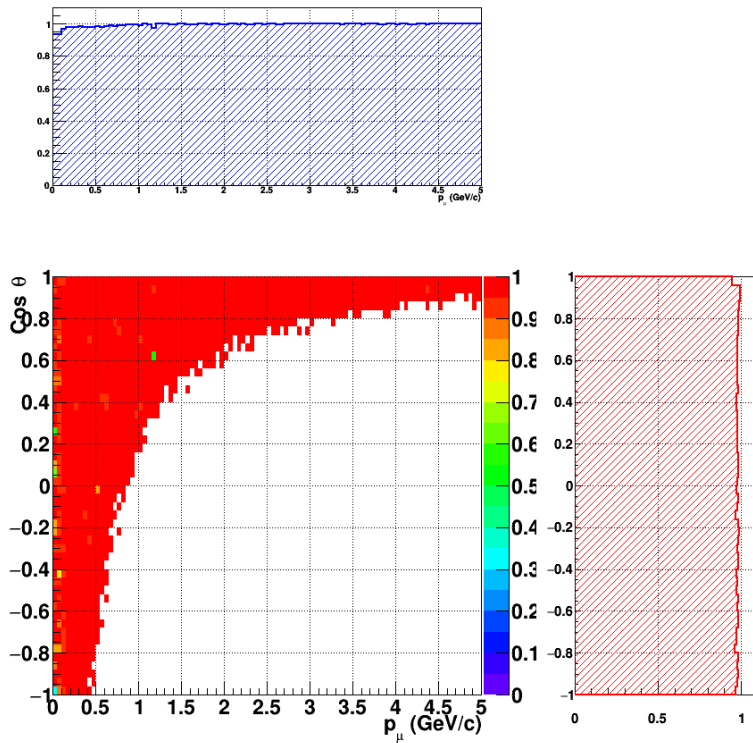


Figure 29: Reconstruction efficiency of CC interactions in the WAGASCI empty module as a function of the muon kinematic variables (momentum and angle).

488 **8 Schedule**

489 We would like to start a physics data taking from T2K beam time after the summer
490 shutdown in 2018. By then, commissioning and tests of the detectors will be completed
491 in J-PARC T59. The experiment can run parasitically with T2K, therefore we request no
492 dedicated beam time nor beam condition as discussed in the following section.

493 Once the approved POT is accumulated, the WAGASCI modules will be removed
494 from the experimental site, but we would like to keep the Baby-MIND and the Side-MRD
495 modules on the B2 floor of the NM pit as common platforms of future neutrino experiments
496 using the T2K neutrino beam.

497 **9 Requests**

498 **9.1 Neutrino beam**

499 The experiment can run parasitically with T2K, therefore we request no dedicated beam
500 time nor beam condition. As data taking periods, we request the ‘nominal’ T2K one-year
501 operation both for the neutrino beam and the antineutrino beam. The T2K has been
502 requesting 0.9×10^{21} POT/year and actually accumulating about 0.7×10^{21} POT/year in
503 recent years. For each year, starting from the Autumn, T2K is running predominantly in
504 the neutrino mode or in the antineutrino mode. Our request is to have one-year neutrino-
505 mode data and another one-year antineutrino mode data assuming that the POT for the
506 fast extraction in each year is more than 0.5×10^{21} POT.

507 **9.2 Equipment request including power line**

508 We request the followings in terms of equipment on the B2 floor:

- 509 • Site for the WAGASCI modules, Side-MRD modules and BabyMIND and their elec-
510 tronics system on the B2 floor of the near detector hall (Fig. 2).
- 511 • Anchor points (holes) on the B2 floor to secure the WAGASCI modules, Side-MRD
512 module and Baby-MIND (Fig. ??)
- 513 • Power line for the magnets in Baby-MIND: 400 V tri-phase 48-to-62 Hz, capable of
514 delivering 12 kW.
- 515 • Electricity for electronics and water circulation system, 3 kW, standard Japanese
516 electrical sockets.
 - 517 1. Online PCs: 2.1 kW
 - 518 2. Electronics: 0.7 kW
 - 519 3. Water sensors: ?

- 520 • Air conditioner for cooling heat generation at Baby-MIND magnets, online PCs and
521 electronics
- 522 • Beam timing signal and spill information
- 523 • Network connection

524 **10 Conclusion**

525 **References**

- 526 [1] K. Abe et al. Measurement of the muon neutrino inclusive charged-current cross sec-
527 tion in the energy range of 13 GeV with the T2K INGRID detector. *Phys. Rev.*,
528 D93(7):072002, 2016.